

Reconstructing spectral functions via automatic differentiation

Lingxiao Wang,¹ Shuzhe Shi,^{2,3,*} and Kai Zhou^{1,†}

¹Frankfurt Institute for Advanced Studies, Ruth Moufang Strasse 1, D-60438, Frankfurt am Main, Germany

²Department of Physics, McGill University, Montreal, Quebec H3A 2T8, Canada.

³Center for Nuclear Theory, Department of Physics and Astronomy, Stony Brook University, Stony Brook, New York, 11784, USA.

(Dated: November 30, 2021)

Reconstructing spectral functions from Euclidean Green’s functions is an important inverse problem in many-body physics. However, the inversion is proved to be ill-posed in the realistic systems with noisy Green’s functions. In this Letter, we propose an automatic differentiation(AD) framework as a generic tool for the spectral reconstruction from propagator observable. Exploiting the neural networks’ regularization as a non-local smoothness regulator of the spectral function, we represent spectral functions by neural networks and use propagator’s reconstruction error to optimize the network parameters unsupervisedly. In the training process, except for the positive-definite form for the spectral function, there is no other explicit physical priors embedded into the neural networks. The reconstruction performance is assessed through relative entropy and mean square error for two different network representations. Compared to the maximum entropy method, the AD framework achieves better performance in large-noise situation. It is noted that the freedom of introducing non-local regularization is an inherent advantage of the present framework and may lead to substantial improvements in solving inverse problems.

Introduction. The numerical solution to inverse problems is a vital area of research in many domains of science. In physics, especially quantum many-body systems, it’s necessary to perform an analytic continuation of function from finite observations which however is ill-posed [1, 2]. It is encountered for example, in Euclidean Quantum Field Theory (QFT) when one aims at rebuilding spectral functions based on some discrete data points along the Euclidean axis. More specifically, the inverse problem occurs when we take a non-perturbative Monte Carlo simulations (e.g., lattice QCD) and try to bridge the propagator data points with physical spectral [3]. The knowledge of spectral function will be further applied in transport process and non-equilibrium phenomena in heavy ion collisions [3, 4].

In general, the problem set-up is from a Fredholm equation of the first kind, which takes the following form,

$$g(t) = K \circ f := \int_a^b K(t, s) f(s) ds, \quad (1)$$

and the problem is to reconstruct the function $f(s)$ given the continuous kernel function $K(t, s)$ and the function $g(t)$. In realistic systems, $g(t)$ is often available in a discrete form numerically. When dealing with a finite set of data points with non-vanishing uncertainty, the inverse transform becomes ill-conditioned or degenerated [5, 6]. Regarding the convolution kernel as a linear operator, it can be expanded by basis functions in a Hilbert space. Refs. [7] and [8] respectively show that kernels of Laplace transformation, ($K(t, s) = e^{-st}$), and Källén–Lehmann(KL) transformation, ($K(t, s) = s(s^2 + t^2)^{-1} \pi^{-1}$), have eigenvalues with arbitrarily small magnitude, and their corresponding eigenfunctions — referred to as *null-modes* — induce negligible changes

in function $g(t)$. Meanwhile, the null-modes correspond to arbitrarily large eigenvalues of the inversion operator. Therefore the inversion is numerically unstable when reconstructing $f(s)$ from a noisy $g(t)$. In Fig. 1, we show examples of different $f(s)$ functions(at left hand side) that correspond to $g(t)$ functions with negligible differences(at right hand side).

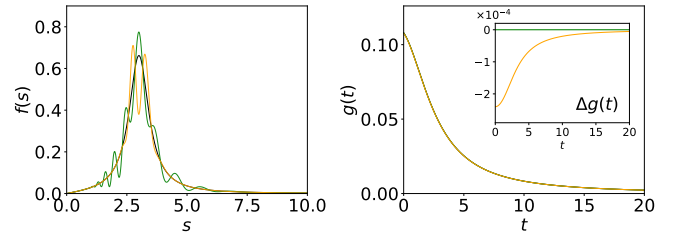


FIG. 1. Spectral functions differed by null-modes (left) and their corresponding Källén–Lehmann correlation functions (right). The insert figure shows the differences-in-propagator caused by null-modes.

Many efforts have been made to break the degeneracy by adding regulator terms inside the inversion process, such as the Tikhonov regularization [6, 9]. In past two decades, the most common approach in such reconstruction task is statistical inference. It comprises prior knowledge from physical domains to regularize the inversion [3, 10, 11]. As one classical paradigm, introducing Shannon–Jaynes entropy regularizes the reconstruction to an unique solution with suppressing null-modes [12–14], that is the maximum entropy method (MEM) [1, 3]. In general, the MEM addresses this problem by regularization of the least-squares fit with an entropy term $S[f] = - \int ds [f(s) - m(s) - f(s) \ln(f(s)/m(s))]$. Standard optimizations aim to maximize $Q[f] = \chi^2[f]/2 -$

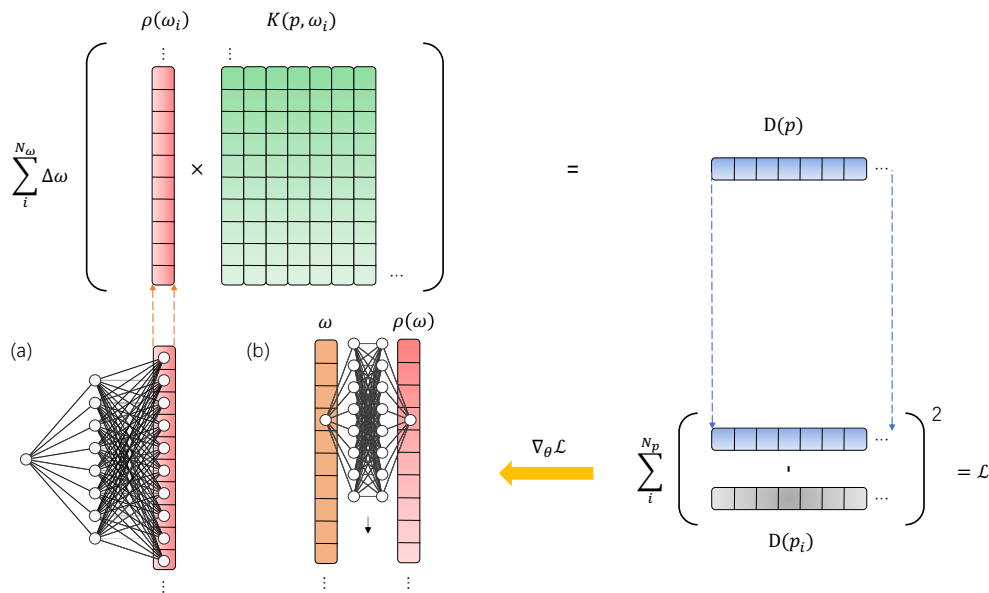


FIG. 2. Automatic differentiation framework to reconstruct spectral from observations. (a) **NN**. Neural networks have outputs as a list representation of spectrum $\rho_i(\omega_i)$. (b) **NN-P2P**. Neural networks have input and output nodes as (ω_i, ρ_i) pairwise.

$\alpha S[f]$ through changing $f(s)$ guided by a prior model $m(s)$, where α is a positive parameter that weights the relative importance between the entropy and the error terms. Although both Tikhonov and Shannon–Jaynes regularization terms yield unique solution of $f(s)$, it is not guaranteed that the reconstructed $f(s)$ is the physical one. Besides, there are some studies employing supervised approaches to train deep neural networks (DNNs) for learning the inverse mapping [15–19]. In these works, the prior knowledge is encoded in amounts of training data from specific physics insights, whereas one should be careful about the risk that biases might be introduced in training set. Efforts have been made in unbiased reconstructions by designing physics-informed networks and using complete basis to prepare training data sets [19]. Besides, to alleviate the dependence on specific kinds of training data, there are also studies adopting the radial basis functions and Gaussian process [20, 21] to perform the inversion directly.

In this Letter, we propose an unsupervised automatic differentiation (AD) approach to solve a spectral reconstruction task without training data preparation. Noting the oscillation caused by null-modes, it is natural to add smoothness condition to regularize the degeneracy. Therefore, we represent spectral functions by artificial neural networks (ANNs), in which the ANNs can preserve smoothness automatically. The universal approximation theorem ensures that ANNs can approximate any kind of continuous function with nonlinear activation functions [22, 23]. We focus on the quality of the spectral function reconstructed from inverting the KL convolu-

tion [24],

$$D(p) = \int_0^\infty K(p, \omega) \rho(\omega) d\omega \equiv \int_0^\infty \frac{\omega \rho(\omega)}{\omega^2 + p^2} \frac{d\omega}{\pi}, \quad (2)$$

where $D(p)$ is a propagator derived from a given spectral function $\rho(\omega)$. It is related to a wide range of quantum many-body systems, yet proved to be difficult to solve satisfactorily [13, 14]. It shall be worth noting that the framework discussed herein may be applied to other ill-conditioned kernels even extended to different tasks.

Automatic Differentiation. Fig. 2 shows the flow chart of the devised AD framework with network representations to reconstruct spectral from propagator observable. The output of network representations are $\vec{\rho} = [\rho_1, \rho_2, \dots, \rho_{N_\omega}]$, from which we can calculate the propagator as $D(p) = \sum_i^{N_\omega} K(p, \omega_i) \rho_i \Delta\omega$. As Fig. 2 shows, after the forward process of the network and convolution, we can get the spectral $\vec{\rho}$ and further the correlators' reconstruction error as loss function,

$$\mathcal{L} = \sum_i^{N_p} w_i (D_i - D(p_i))^2, \quad (3)$$

where D_i is observed data at p_i , and w_i denote extra weights of each observation. When taking the inverse variance as w_i , Eq. (3) becomes the standard χ^2 function. Meanwhile, one can directly extend it to multiple data points by making summation over them with calculating all variances. To optimize the parameters of network representations $\{\theta\}$ with loss function, we im-

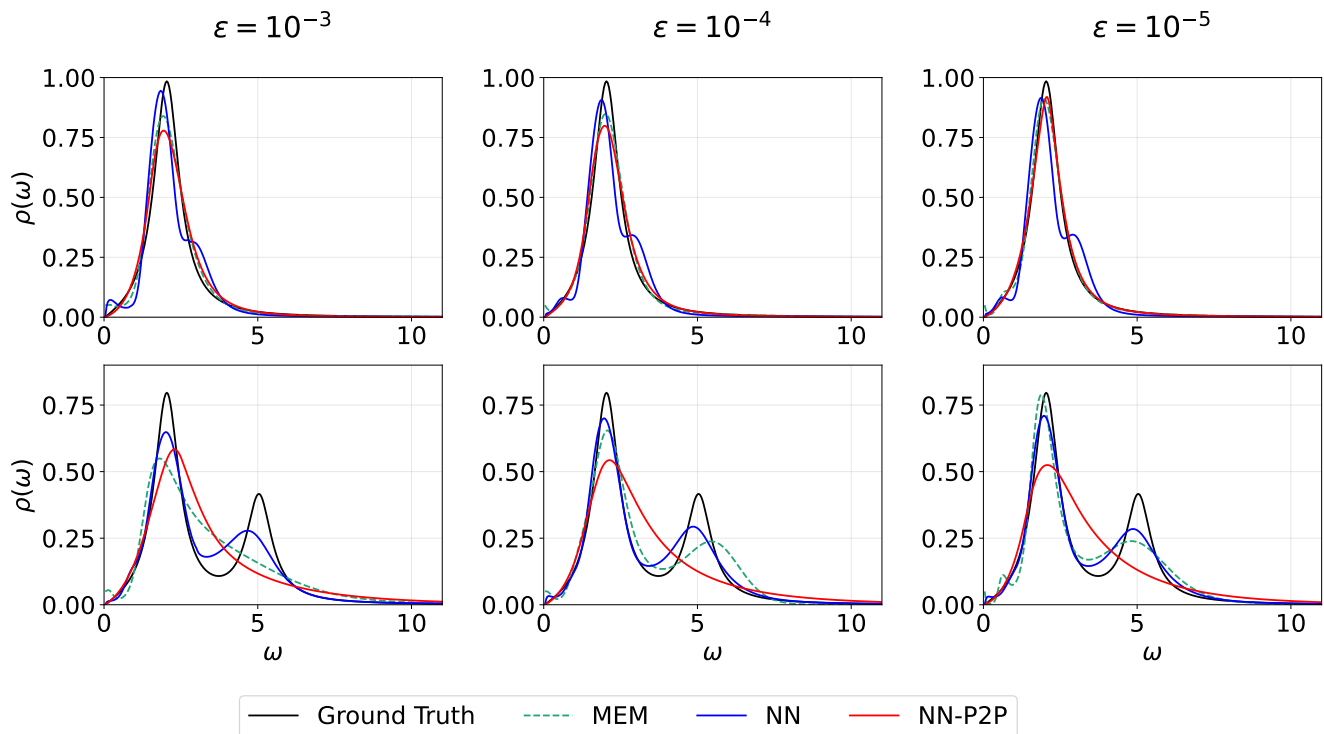


FIG. 3. The predicted spectral functions from MEM, NN and NN-P2P. From left to right panels, different Gaussian noises are added to the propagator spectral data with $\varepsilon = 10^{-3}, 10^{-4}, 10^{-5}$.

plement gradient-based algorithms. It derives as,

$$\nabla_{\theta} \mathcal{L} = \sum_{j,k} K(p_j, \omega_k) \frac{\partial \mathcal{L}}{\partial D(p_j)} \nabla_{\theta} \rho_k, \quad (4)$$

where $\nabla_{\theta} \rho_k$ is computed by the standard backward propagation (BP) method in deep learning [22]. The reconstruction error will be transmitted to each layer of neural networks, combined with gradients derived from automatic differentiation [25], they are used to optimize the parameters of neural networks. In our case, the Adam optimizer is adopted in following computations. It is a stochastic gradient-based algorithm that is based on adaptive estimations of first-order and second-order moments [26].

Neural network representations. As Fig. 2 shown, we develop two representations with different levels of non-local correlations among $\rho(\omega_i)$'s to represent the spectral functions with artificial neural networks (ANNs). The first is demonstrated as Fig. 2(a) and named as NN, in which we use L -layers neural network to represent in list format the spectral function $\rho(\omega)$ with a constant input node $a^0 = C$ and multiple output nodes $a^L = [\rho_1, \rho_2, \dots, \rho_{N_\omega}]$. The width of the l -th layer inside the network is n_l , to which the associated weight parameters control the correlation among the discrete outputs in a concealed form. In a special case, a discrete list of ρ_i itself is equivalent to set $L = 1$ without any bias nodes, meanwhile, the differentiable variables are directly ele-

ments of $\vec{\rho}$ as network weights. If one approximates the integration over frequencies ω_i to be summation over N_ω points at fixed frequency interval $d\omega$, then it is suitable to the vectorized AD framework described above. The second representation with ANNs is shown as Fig. 2(b), where the input node is $a^0 = \omega$ and the output node is interpreted to be $a^L = \rho(\omega)$. It is termed as point-to-point neural networks (abbreviated as NN-P2P) and it consists of finite first-order differentiable modules, in which the continuity of function $\rho(\omega)$ is naturally preserved [23, 27].

For the optimization of the neural network representations, we adopt the Adam optimizer with L_2 regularization, which is a summation over the L_2 norm of all differentiable weight parameters for the network, $L_2 = \lambda \sum_i (\theta_{W,i})^2$. The smoothness regulator is implemented only for NN, which derives as $L_s = \lambda_s \sum_{i=1}^{N_\omega} (\rho_i - \rho_{i-1})^2$. In training process, we obey an annealing strategy which set a tight regularization in the beginning and loosen it repeatedly in first 20000 epochs. After that, early stopping is applied for the training with the criterion to be when error between observed $D(p)$ and reconstructed $D(p)$ does not decrease, or the whole training exceeds 50000 epochs. The L_2 regularization set as $\lambda = 10^{-3}$ and learning rate is 10^{-2} for all cases. The initial smoothness regulator of NN is $\lambda_s = 10^{-3}$. Besides, the physical prior we embedded into these representations is the positive-definiteness of fermionic spectral functions (in

Lattice QCD case, they are hadronic spectra), which is introduced by applying *Softplus* activation function at output layer as $\sigma(x) = \ln(1 + e^x)$.

Reconstruction performance. — In this section, we demonstrate the performance of our framework by testing their quality in reverting the Green’s functions of known spectral functions (aka. mock data). We start with a superposed collection of Breit–Wigner peaks, which is based on a parametrization obtained directly from one-loop perturbative quantum field theory [15, 28]. Each individual Breit–Wigner spectral function is given by,

$$\rho^{(\text{BW})}(\omega) = \frac{4A\Gamma\omega}{(M^2 + \Gamma^2 - \omega^2)^2 + 4\Gamma^2\omega^2}. \quad (5)$$

Here M denotes the mass of the corresponding state, Γ is its width and A amounts to a positive normalization constant. The multi-peak structure is built by combining different single peak modules together.

Two profiles of spectral functions from Eq. (5) are set as ground truths. In Fig. 3, the upper is from a single peak spectrum with $A = 1.0, \Gamma = 0.5, M = 2.0$ (hereunder in paper, we omit the energy unit of mass M , width Γ , frequency ω and momentum p) and the below one is from double peak profile with $A_1 = 0.8, A_2 = 1.0, \Gamma_1 = \Gamma_2 = 0.5, M_1 = 2.0, M_2 = 5.0$. To imitate the realistic observable data, we add noise to the mock data with $\tilde{D}_i = D(p_i) + n_\varepsilon$, where the noise term follows normal distribution with variance ε^2 , $P(n_\varepsilon) = \mathcal{N}(0, \varepsilon^2)$. In Fig. 3, we compare the reconstruction results with $\varepsilon = 10^{-3}, 10^{-4}, 10^{-5}$, respectively. The two network representations are marked by blue and red lines. They all show remarkable reconstruction performances for a single peak at each noise level. As a comparison, results from MEM are also shown as green lines. We see that, MEM show oscillations around zero-point under different noise backgrounds. The rebuilding spectral function from **NN-P2P** do not oscillate. This is especially important for such a task of extracting the transport coefficients from real-world lattice calculation data [3, 15].

For mock data with two peaks, we observe that the smoothness condition of **NN-P2P** erroneously suppress the bimodal structure, whereas **NN** successfully unfolds the two peaks information from Green’s functions even with noise $\varepsilon = 10^{-3}$. Although **NN-P2P** misses the second peak which may appear in the case of bimodal, the calculations of different order momentum from spectral function will not be disturbed. Another advantage of the **NN-P2P** architecture is its the stable performance of the spectral function at small ω limit, which is important for the measurement of conductivity $\sigma \equiv \lim_{\omega \rightarrow 0} \rho(\omega)/\omega$ [29, 30]. The smoothness condition automatically encoded in the network set-up suppresses the oscillating null-modes especially at small frequency region, and therefore allows the reliable extraction of conductivity in **NN-P2P**.

In Fig. 4, two reconstruction performance are demonstrated for an ideal noise-free case with two net-

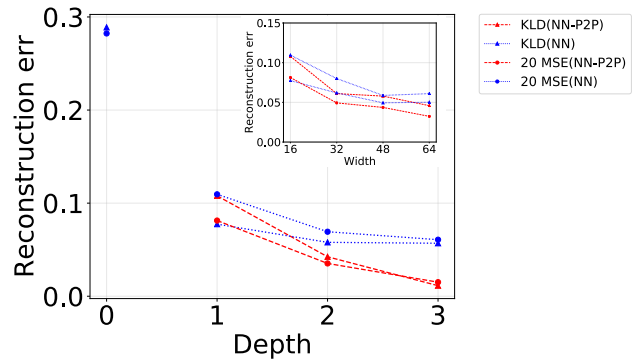


FIG. 4. Mean square error (dot) and relative entropy (dash) with different hidden layers (width = 16), in which “depth = 0” means list representation without hidden layers. The insert is estimators with different widths of neural networks (depth = 1).

work representations. The results are on the single peak case described in following section. The integral form of MSE derives as $\int_0^\infty (\tilde{\rho}(\omega) - \rho(\omega))^2 d\omega$ and the relative entropy (or Kullback–Leibler divergence) is $\int_0^\infty \rho(\omega) \log(\rho(\omega)/\tilde{\rho}(\omega)) d\omega$, where $\tilde{\rho}(\omega)$ is ground truth spectral function and $\rho(\omega)$ is the reconstructed from neural networks. The performance of two representations remain good enough after setting width = 64 and depth = 3, which is adopted as our parameter setting in whole paper.

Summary. — We present an automatic differentiation framework as a generic tool for unfolding spectral functions from observable data. The representations of spectral functions are with two different neural network architectures, in which non-local smoothness regularization and modern optimization algorithm are implemented conveniently. We demonstrated the validity of our framework on mock examples from Breit–Wigner spectral functions with single and two peaks. To account for uncertainties from numerical simulation for the propagator observations, we confronted the framework in different levels of noise contamination for the observations. Compared to conventional MEM calculations, our framework shows superior performance especially in two peaks situation with larger noise. Also, the **NN-P2P** representation gives smooth and well-matched low frequencies spectral behavior, which is important in extracting transport properties for the system. Although the inverse problems cannot be fully-solved in our framework, the remarkable performances of reconstructing spectral functions suggest that the framework and the freedom of introducing non-local regularization are inherent advantages of the present approach and may lead to improvements in solving the inverse problem in the future.

Acknowledgment. — We thank Drs. Heng-Tong Ding, Swagato Mukherjee and Gergely Endrödi for helpful discussions. The work is supported by (i) the BMBF un-

der the ErUM-Data project (K. Z.), (ii) the AI grant of SAMSON AG, Frankfurt (K. Z. and L. W.), (iii) Natural Sciences and Engineering Research Council of Canada (S. S.), (iv) the Bourses d'excellence pour étudiants étrangers (PBEEE) from Le Fonds de Recherche du Québec - Nature et technologies (FRQNT) (S. S.), (v) U.S. Department of Energy, Office of Science, Office of Nuclear Physics, grant No. DE-FG88ER40388 (S. S.). K. Z. also thanks the donation of NVIDIA GPUs from NVIDIA Corporation.

* shuzhe.shi@stonybrook.edu

† zhou@fias.uni-frankfurt.de

- [1] M. Jarrell and J. E. Gubernatis, *Physics Reports* **269**, 133 (1996).
- [2] S. I. Kabanikhin, *Inverse and Ill-Posed Problems: Theory and Applications* (De Gruyter, 2011).
- [3] M. Asakawa, T. Hatsuda, and Y. Nakahara, *Prog. Part. Nucl. Phys.* **46**, 459 (2001), [arXiv:hep-lat/0011040](https://arxiv.org/abs/hep-lat/0011040).
- [4] A. Rothkopf, *PoS Confinement2018*, 026 (2018), [arXiv:1903.02293](https://arxiv.org/abs/1903.02293) [hep-ph].
- [5] P. J. Caudrey, *Physica D: Nonlinear Phenomena* **6**, 51 (1982).
- [6] A. N. Tikhonov, A. V. Goncharsky, V. V. Stepanov, and A. G. Yagola, *Numerical Methods for the Solution of Ill-Posed Problems* (Springer Netherlands, Dordrecht, 1995).
- [7] J. G. McWhirter and E. R. Pike, *Journal of Physics A Mathematical General* **11**, 1729 (1978).
- [8] S. Shi, L. Wang, and K. Zhou, in progress (2021).
- [9] M. Bertero, in *Advances in Electronics and Electron Physics*, Vol. 75, edited by P. W. Hawkes (Academic Press, 1989) pp. 1–120.
- [10] Y. Burnier and A. Rothkopf, *Phys. Rev. Lett.* **111**, 182003 (2013), [arXiv:1307.6106](https://arxiv.org/abs/1307.6106) [hep-lat].
- [11] Y. Burnier, O. Kaczmarek, and A. Rothkopf, *Phys. Rev. Lett.* **114**, 082001 (2015), [arXiv:1410.2546](https://arxiv.org/abs/1410.2546) [hep-lat].
- [12] R. K. Bryan, *Eur. Biophys. J.* **18**, 165 (1990).
- [13] M. Asakawa, (2020), [arXiv:2001.10205](https://arxiv.org/abs/2001.10205) [hep-ph].
- [14] A. Rothkopf, *Data* **5**, 85 (2020).
- [15] L. Kades, J. M. Pawłowski, A. Rothkopf, M. Scherzer, J. M. Urban, S. J. Wetzel, N. Wink, and F. P. G. Ziegler, *Phys. Rev. D* **102**, 096001 (2020), [arXiv:1905.04305](https://arxiv.org/abs/1905.04305) [physics.comp-ph].
- [16] H. Yoon, J.-H. Sim, and M. J. Han, *Phys. Rev. B* **98**, 245101 (2018), [arXiv:1806.03841](https://arxiv.org/abs/1806.03841) [cond-mat.str-el].
- [17] R. Fournier, L. Wang, O. V. Yazyev, and Q. Wu, *Phys. Rev. Lett.* **124**, 056401 (2020).
- [18] H. Li, J. Schwab, S. Antholzer, and M. Haltmeier, *Inverse Problems* **36**, 065005 (2020).
- [19] S. Y. Chen, H. T. Ding, F. Y. Liu, G. Papp, and C. B. Yang, (2021), [arXiv:2110.13521](https://arxiv.org/abs/2110.13521) [hep-lat].
- [20] M. Zhou, F. Gao, J. Chao, Y.-X. Liu, and H. Song, *Phys. Rev. D* **104**, 076011 (2021), [arXiv:2106.08168](https://arxiv.org/abs/2106.08168) [hep-ph].
- [21] J. Horak, J. M. Pawłowski, J. Rodríguez-Quintero, J. Turnwald, J. M. Urban, N. Wink, and S. Zafeiropoulos, (2021), [arXiv:2107.13464](https://arxiv.org/abs/2107.13464) [hep-ph].
- [22] I. Goodfellow, Y. Bengio, and A. Courville, *Deep Learning* (MIT Press, 2016).
- [23] L. Wu, Z. Zhu, and W. E, arXiv e-prints , [arXiv:1706.10239](https://arxiv.org/abs/1706.10239) (2017), [arXiv:1706.10239](https://arxiv.org/abs/1706.10239) [cs.LG].
- [24] M. E. Peskin and D. V. Schroeder, *An Introduction To Quantum Field Theory*, first edition edition ed. (Westview Press, Reading, Mass, 1995).
- [25] It can be conveniently implemented in many deep learning frameworks. In our case, main computations are deployed in Pytorch but also validated in Tensorflow.
- [26] D. P. Kingma and J. Ba, arXiv e-prints , [arXiv:1412.6980](https://arxiv.org/abs/1412.6980) (2014), [arXiv:1412.6980](https://arxiv.org/abs/1412.6980) [cs.LG].
- [27] M. Rosca, T. Weber, A. Gretton, and S. Mohamed, in *Proceedings on "I Can't Believe It's Not Better!" At NeurIPS Workshops*, Proceedings of Machine Learning Research, Vol. 137, edited by J. Zosa Forde, F. Ruiz, M. F. Pradier, and A. Schein (PMLR, 2020) pp. 21–32.
- [28] R.-A. Tripolt, P. Gubler, M. Ulybyshev, and L. Von Smekal, *Comput. Phys. Commun.* **237**, 129 (2019), [arXiv:1801.10348](https://arxiv.org/abs/1801.10348) [hep-ph].
- [29] H.-T. Ding, F. Karsch, and S. Mukherjee, *Int. J. Mod. Phys. E* **24**, 1530007 (2015), [arXiv:1504.05274](https://arxiv.org/abs/1504.05274) [hep-lat].
- [30] C. Ratti, *Rept. Prog. Phys.* **81**, 084301 (2018), [arXiv:1804.07810](https://arxiv.org/abs/1804.07810) [hep-lat].